Published in final edited form as:
Biochemistry. 2008 September 9; 47(36): 9497–9504. doi:10.1021/bi800971v.

Structure of Diethyl Phosphate Bound to the Binuclear Metal Center of Phosphotriesterase†

Jungwook Kim[§], **Ping-Chuan Tsai**[‡], **Shi-Lu Chen**[Ψ], **Fahmi Himo**[Ψ,*], **Steven C. Almo**[§,*], and **Frank M. Raushel**[‡,*]

[§]Albert Einstein College of Medicine, 1300 Morris Park Avenue, Bronx, New York 10461

[‡]Department of Chemistry, P.O. Box 30012, Texas A&M University, College Station, Texas 77842-3012

[Ψ] Department of Theoretical Chemistry, School of Biotechnology, Royal Institute of Technology, 10691 Stockholm, Sweden.

Abstract

The bacterial phosphotriesterase (PTE) from *Pseudomonas diminuta* catalyzes the hydrolysis of organophosphate esters at rates close to the diffusion limit. X-ray diffraction studies have shown that a binuclear metal center is positioned in the active site of PTE and that this complex is responsible for the activation of the nucleophilic water from solvent. In this paper the three dimensional structure of PTE was determined in the presence of the hydrolysis product, diethyl phosphate (DEP), and a product analogue, cacodylate. In the structure of the PTE-diethyl phosphate complex the DEP product is found symmetrically bridging the two divalent cations. The DEP displaces the hydroxide from solvent that normally bridges the two divalent cations in structures determined in the presence or absence of substrate analogues. One of the phosphoryl oxygen atoms in the PTE-DEP complex is 2.0 Å away from the α-metal ion while the other oxygen is 2.2 Å away from the β-metal ion. The two metal ions are separated by a distance of 4.0 Å. A similar structure is observed in the presence of cacodylate. Analogous complexes have previously been observed for the product complexes of isoaspartyl dipeptidase, D-aminoacylase, and dihydroorotase from the amidohydrolase superfamily of enzymes. The experimentally determined structure of the PTE-diethyl phosphate product complex is inconsistent with a recent proposal based upon QM/MM simulations which postulated the formation of an asymmetrical product complex bound exclusively to the β-metal ion with a metal-metal separation of 5.3 Å. This structure is also inconsistent with a chemical mechanism for substrate hydrolysis that utilizes the bridging hydroxide as a base to abstract a proton from a water molecule loosely associated with the α-metal ion. Density functional theory (DFT) calculations support a reaction mechanism that utilizes the bridging hydroxide as the direct nucleophile in the hydrolysis of organophosphate esters by PTE.

†This work was supported in part by the NIH (GM71790 and GM68550) and the Robert A. Welch Foundation (A-840). JK was supported by GM76988. FH acknowledges financial help from The Swedish National Research Council and The Carl Trygger Foundation.

*To whom correspondence may be sent: (FMR) telephone: (979) 845-3373; fax: (979)-845-9452; e-mail: raushel@tamu.edu (SCA) telephone: (718) 430-2746; fax: (718)-430-8565; e-mail: almo@aecom.yu.edu (FH) telephone: 46-8-55378415; fax: 46-8-55378590; e-mail: himo@theochem.kth.se.

The X-ray coordinates and structure factors have been deposited in the Protein Data Bank (PDB codes: 2O4Q and 3CAK).

Supporting information available

Electron density for cacodylate bound to the active site of G60A (Figure S1) and for diethyl phosphate bound to wild type PTE (Figures S2A and S2B). This material is available free of charge via the Internet at http://pubs.acs.org.

The amidohydrolase superfamily (AHS[1]) of enzymes catalyzes hydrolytic, decarboxylation, isomerization, and hydration reactions within carbohydrate, nucleic acid and amino acid based substrates (1). Most of the structurally characterized enzymes of the AHS contain either a binuclear or mononuclear metal center embedded at the C-terminal end of a $(\beta/\alpha)_8$-barrel structural domain. For those enzymes that catalyze hydrolytic reactions the metal centers have been shown to activate solvent water for nucleophilic attack. High resolution x-ray structures have been obtained for approximately 20 members of the AHS and in these enzymes the metal centers are naturally populated by zinc, iron or nickel (1). In addition, some members of the AHS are also active with manganese, cobalt, or cadmium (2). Perhaps the best characterized member of the amidohydrolase superfamily is the bacterial phosphotriesterase from *Pseudomonas diminuta* (3).

Phosphotriesterase (PTE) catalyzes the hydrolysis of a wide range of organophosphate esters, including agricultural pesticides and highly toxic chemical warfare agents (3-5). A natural substrate for PTE is not known, however, the purified PTE exhibits a remarkable catalytic activity towards the hydrolysis of the commercial pesticide, paraoxon. Kinetic constants for k_{cat} and k_{cat}/K_m of $10^4\ s^{-1}$ and $10^8\ M^{-1}\ s^{-1}$, respectively, have been measured for the hydrolysis of this substrate (6,7). The reaction for the hydrolysis of paraoxon is presented in Scheme 1. The enzyme has been crystallized and high resolution x-ray structures of the Zn/Zn-, Cd/Cd-, Mn/Mn- and the Zn/Cd-PTE hybrid have been solved (2). Shown in Figure 1 is the coordination scheme for the binuclear metal center of Cd/Cd-PTE. The more solvent shielded metal (M_α) is coordinated to His-55, His-57, and Asp-301, whereas the more solvent-exposed metal (M_β) is coordinated to His-201, His-230 and two water molecules from solvent. The two metals are bridged to one another by a carboxylated lysine (Lys-169) and hydroxide. The bridging hydroxide is additionally hydrogen bonded to the side chain carboxylate of Asp-301.

The reaction mechanism for the hydrolysis of organophosphate triesters by phosphotriesterase has received considerable experimental and computational attention (8-11). Presented in Scheme 2 is a slightly modified reaction mechanism, originally proposed by Aubert *et al*., for the hydrolysis of paraoxon by the phosphotriesterase from *P. diminuta* (8). In this mechanism the organophosphate substrate binds to the active site with the displacement of a water molecule from the β-metal ion. The interaction of the substrate with the β-metal ion weakens the coordination of the bridging hydroxide to the β-metal ion and facilitates the nucleophilic attack of the hydroxide in an S_N2-like reaction on the phosphorus center of the substrate. The bond to the leaving group phenol is broken and the single proton from the nucleophilic hydroxide is transferred to Asp-301. The anionic diethyl phosphate is bound within the active site as a bridging ligand between the two divalent cations. The diethyl phosphate dissociates from the active site and the binuclear metal center is subsequently recharged for another round of catalysis.

Experimental evidence for the direct interaction of the substrate with the β-metal ion comes from the x-ray structure of PTE bound with a diisopropyl methyl phosphonate inhibitor (PDB code 1EZ2) and the differential effects on the kinetic constants for the hydrolysis of phosphate and thiophosphate esters with zinc and cadmium substituted variants of PTE (8). Support for the weakening of the interaction of the bridging hydroxide with the β-metal ion is derived from the loss of antiferromagnetic coupling between the two metal ions in Mn/Mn-PTE upon binding of substrate analogues using EPR spectroscopy (12). The utilization of the hydroxide that is bridging the two metal ions as the direct nucleophile is supported by the observation that in the presence of substrate analogues there are no other water molecules bound to either of the two metal ions in Zn/Zn-PTE.

[1]Abbreviations: AHS, amidohydrolase superfamily; DFT, density functional theory; PTE, phosphotriesterase, DEP, diethyl phosphate.

General support for the reaction mechanism of Scheme 2 was also provided by recent density functional theory (DFT) calculations by Chen *et al.* (9). A model of the PTE active site was devised based on the crystal structure of the wild-type Zn/Zn-enzyme (PDB code 1HZY). The calculations showed that the bridging hydroxide is sufficiently nucleophilic to attack the phosphorus center of organophosphate triester substrates.

Recently, two provocative modifications to the mechanism presented in Scheme 2 have been proposed (10,11). In a computational assessment of the PTE reaction mechanism, Wong and Gao have postulated a mononuclear coordination scheme of protonated diethyl phosphate to the β-metal ion that is coupled with a lengthening of the metal-metal distance from 3.6 Å to 5.3 Å as the reaction proceeds from an enzyme-substrate complex to an enzyme-product complex (10). A representation of this product complex is provided in Scheme 3. In addition, Ollis and colleagues have proposed that the bridging hydroxide acts not as a nucleophile but as a base in the abstraction of a proton from a water molecule that is apparently loosely coordinated to the α-metal ion. The chemical mechanism and product complex proposed by Ollis and colleagues are illustrated in Scheme 3 (11). Experimental support for this proposal derives primarily from an x-ray structure of a dimethyl thiophosphate complex of the PTE from *Agrobacterium radiobacter* and catalytic properties of model complexes that are purported to mimic the active site of PTE (13).

In this investigation we have utilized x-ray diffraction techniques to probe the structure of diethylphosphate bound to the active site of PTE. This structure has been used to help differentiate among the three mechanistic possibilities for the hydrolysis of organophosphate esters by PTE. In addition, we have performed DFT calculations to assess the energetic feasibility of the base mechanism proposed by Ollis and co-workers.

Materials and Methods

Purification of Wild-Type and G60A Mutant

The genes encoding the wild-type PTE and the G60A mutant were ligated between the *Nde*I and *Eco*RI sites of a pET20b (+) plasmid. The wild-type and mutant plasmids were transformed into *E. coli* strain BL-21 cells (DE3) (7). The transformed BL-21cells were inoculated in Luria-Bertani (LB) broth overnight at 37 °C. The overnight cultures were then incubated in Terrific Broth (TB) containing 100 μg/mL ampicillin and 1.0 mM $CoCl_2$ at 30 °C. IPTG was added when the OD_{600} reached 0.4, followed by incubation for 36-42 hours at 30 °C to reach the stationary phase. The cell paste was harvested by centrifugation at 4 °C. The wild-type PTE and G60A mutant were purified as previously described (8). SDS-polyacrylamide gel electrophoresis demonstrated that the wild-type PTE and the G60A mutant migrated with proteins having a molecular weight of ~36 kDa. The purity was estimated to be greater than 95%.

Measurement of Kinetic Constants

The kinetic parameters were obtained by fitting the data to equation 1, where v is the initial velocity, k_{cat} is the turnover number, [A] is the substrate concentration, E_t is the enzyme concentration, and K_a is the Michaelis constant. The inhibition constants, K_{ii} and K_{is}, for the noncompetitive inhibition of cacodylate in the presence of the substrate paraoxon, were determined by fitting the data to equation 2, where [I] is the concentration of inhibitor and the other constants have been defined previously. The concentration of paraoxon was varied from 0.05 mM to 2.5 mM. Six different cacodylate concentrations were used in these assays, ranging from 0 to 250 mM. The rate was measured by following the change in absorbance at 400 nm.

$$v/E_t = k_{cat}[A]/(K_a + [A]) \quad (1)$$

$$v/E_t = k_{cat}[A]/(K_a(1 + ([I]/K_{is})) + [A](1 + ([I]/K_{ii}))) \quad (2)$$

Synthesis of Diethyl Phosphate

Diethyl phosphate was synthesized by Dr. Yingchun Li of Texas A&M University. Diethyl phosphorochloridate was reacted with phenol in ethyl ether in the presence of triethylamine to yield diethyl phenyl phosphate after purification using silica gel chromatography. Hydrogenation of the resulting organophosphate in methanol using Pd/C as a catalyst provided diethyl hydrogen phosphate quantitatively after separation of the catalyst by filtration and removal of the solvent by evaporation under reduced pressure (14). The identity and the purity (>98%) of the diethyl phosphate were confirmed by ^{1}H and ^{31}P NMR spectroscopy.

X-ray Structure Determination and Refinement

The G60A mutant was crystallized by hanging drop vapor diffusion at 21 °C by mixing 1 μL of the protein with 1 μL of reservoir solution (0.2 M magnesium acetate, 0.1 M sodium cacodylate (pH 6.5), 20% polyethylene glycol (PEG 8000)) and equilibrating over 1.0 mL of reservoir solution. X-ray data were collected on a MAR CCD 165 mm detector at the NSLS X3A beam line, using x-ray wavelength at 0.97904 Å and processed with HKL2000 (15). The G60A crystal exhibited diffraction consistent with the space group P_1 (a = 55.29 Å, b = 68.30 Å and c = 90.03 Å; α = 90.05°, β= 100.42°, and γ = 89.96°). There were four G60A molecules (two homodimers) in the asymmetric unit.

The wild-type Co/Co-PTE was co-crystallized with 17 mM diethyl phosphate (DEP) in 0.1 M Bis-Tris (pH 6.5) and 20% PEG monomethyl ether 5000. X-ray data were collected on an R-Axis IV^{++} image plate detector using CuKα radiation from a Rigaku RU-H3R X-ray generator and processed using HKL2000 (15). The co-crystals of wild-type PTE with DEP exhibit diffraction consistent with space group P_1 (a = 43.29 Å, b = 45.34 Å and c = 78.91 Å; α = 104.73°, β = 93.40°, and γ = 97.65°). Two protein molecules were observed in the asymmetric unit.

The structures of G60A and wild-type PTE with bound DEP were determined by molecular replacement using the program MOLREP with 1P6B and 2OB3 as initial search models, respectively (16). Solvent water molecules were built using Arp/ wArp (17). All subsequent model building and refinement was carried out with Coot (18) and REFMAC5 (19). The final models were refined to 1.95 and 1.83 Å with R_{work}/R_{free} of 0.167/0.224 and 0.140/0.196, respectively (Table 1).

Computational Details

All theoretical calculations were performed using the hybrid density functional theory (DFT) B3LYP (20-22). Geometry optimization were carried out with the 6-31G(d,p) basis set for all elements except Zn, for which the effective core potential LANL2DZ basis set was used. Based on these geometries, more accurate energies were obtained by performing single point calculations with the larger basis set 6-311+G(2d,2p) for all elements. Solvation effects were calculated at the same theory level as the optimizations by performing single point calculations on the optimized structures using the CPCM method (23-26). The dielectric constant (ε) was chosen to be 4. Frequency calculations were performed at the same theory level as the

optimizations to obtain zero-point energies (ZPE) and to confirm the nature of the stationary points. All calculations were performed using the Gaussian03 program package (27).

Results

Inhibition by Cacodylate

The kinetic constants of k_{cat}, k_{cat}/K_a, and K_a for the hydrolysis of paraoxon by Co/Co-G60A at pH 9.0 are 2900 s^{-1}, 1.34 × 10^7 M^{-1} s^{-1}, and 210 μM, respectively. The inhibition of Co/Co-G60A was measured using cacodylate as an inhibitor of paraoxon hydrolysis. The double reciprocal plots (data not shown) intersect to the left of the vertical axis and thus cacodylate is a noncompetitive inhibitor versus paraoxon. The kinetic inhibition constants, K_{is} and K_{ii}, determined from fits of the data to equation 2, are 260 ± 100 mM and 110 ± 10 mM, respectively.

Structure of G60A with Cacodylate

The crystals of G60A contain two homodimers in the asymmetric unit. As expected, two metal atoms were found in the active site for each monomer; however, an additional strong feature in the electron density was observed close to the binuclear metal center in all subunits during the refinement. The tetrahedral electron density appeared to interact directly with both metal atoms and was consistent with cacodylate, which was present in the crystallization solution (Supplemental Figure S1). The average B-factors for the main chain protein atoms and cacodylate are 20.52 and 20.70 $Å^2$, respectively. Cacodylate is bound to both metal ions with an average distance of 1.98 ± 0.03 and 2.07 ± 0.06 Å to the α- and β-metal, respectively. The α-metal ion is coordinated to His-55, His-57, and Asp-301 whereas the β-metal ion is coordinated to His-201 and His-230. An image of these interactions is presented in Figure 2. The cacodylate ligand has replaced the bridging hydroxide that has been observed in a number of PTE structures (2). No water molecules are observed to interact with either metal ion in any of the four molecules in the asymmetric unit of the G60A structure. In addition to the two metal ions, cacodylate is within hydrogen bonding distance of Trp-131, the carboxylated Lys-169, His-201, and Asp-301.

Structure of Wild-Ttype PTE with Diethyl Phosphate

Diethyl phosphate (DEP) is the hydrolysis product of paraoxon, the best known substrate for PTE. Various concentrations of DEP, as high as 100 mM, were tested for co-crystallization with wild-type PTE before an optimized condition was determined. In the co-crystals, electron density for DEP was unambiguously located around the binuclear metal site in one subunit (Supplemental Figure S2a). However, the lack of electron density corresponding to one of the two ethyl groups within the ligand was observed in the second subunit (Supplemental Figure 2b). The electron density was modeled as mono ethyl phosphate during the refinement for this subunit. The phosphoryl oxygen atom which is not coordinated to either metal is relatively solvent exposed and the ethyl group occupies a more buried hydrophobic pocket. Subsequent NMR experiments showed that the initial concentration of monoethyl phosphate in the sample of diethyl phosphate was negligible (<1%) and the enzymatic hydrolysis of DEP by PTE was beyond the detection limit even after incubation of PTE with DEP for 5 days (data not shown). These observations suggest that the ethyl group of the second DEP is not observed due to disorder.

With the exception of the missing ethyl group, both ligands of DEP bind in a very similar manner within the binuclear metal center. Therefore, the following discussion will refer only to the first subunit that contains the fully modeled DEP. One of ethyl groups orients toward a hydrophobic patch, composed of Gly-60, Ile-106, Trp-131, and Leu-303. The other ethyl group is more solvent exposed and forms hydrogen bonds through the phosphate ester oxygen with two water molecules. One of the phosphoryl oxygen atoms of DEP is 1.97 Å away from α-

metal ion while the other oxygen is 2.17 Å away the β-metal. The orientation of diethyl phosphate within the active site of PTE is presented in Figure 3. These distances are similar to the orientation of cacodylate in the G60A PTE structure. Moreover, there is no bridging water observed in the binuclear metal site, as a result of the complete displacement by DEP. The DEP ligand is near *N*ε1 of Trp-131, the carboxylate oxygen atoms of the carboxylated Lys-169, and carboxylate oxygen atoms of Asp-301. $N_{\delta 1}$ of His-201 is slightly further away from DEP (3.39 Å) in the structure of the wild type enzyme than from cacodylate (3.19 Å) in the G60A structure.

DFT calculations

To further examine the feasibility of the base mechanism proposed by Ollis and co-workers (11), we have performed DFT calculations using the same model of the Zn/Zn-enzyme active site as in the previous calculations (9). The model is based on the high resolution crystal structure of wild-type Zn/Zn-PTE from *P. diminuta* (PDB code: 1HZY) and consists of the two zinc ions and their first shell ligands, including the bridging hydroxide, the four histidines (His-55, His-57, His-201, His-230), Asp-301, and the carboxylated Lys-169. Hydrogen atoms were added manually and the ligands were truncated so that only side chains were kept in the model. The histidines were thus represented by imidazoles, the aspartate by an acetate, and the carboxylated lysine by a carboxylated methylamine (see Figure 4). Dimethyl 4-nitrophenyl phosphate was chosen as a model substrate, as in the previous study (9). The water molecule, postulated to be the nucleophile in the base mechanism, was added to the model. The model thus consists of 85 atoms and has a total charge of +1.

In the reactant species (Figure 4, React), the phosphoryl oxygen of the substrate binds to the more solvent-exposed β-Zn site and the leaving group is located at the position opposite to the bridging hydroxide. According to the base proposal, the nucleophilic water molecule is bound to the α-Zn. In the calculations, we first placed the water molecule there, but we could not locate a stable conformation with the water bound to the α-Zn. Instead, it dissociates from the Zn during the optimization and forms a hydrogen bond to the bridging hydroxide (see Figure 4, React). From these calculations it can thus be concluded that a hexacoordinate α-Zn is quite unlikely.

We have furthermore optimized the transition state for the nucleophilic attack with the bridging hydroxide acting as a base. The optimized structure is displayed in Figure 4 with important distances indicated. The critical distance between the water oxygen to the phosphorus center (O_W-P) is 1.99 Å. Simultaneously with the O_W-P bond formation, one proton of water molecule is transferred to the bridging oxygen, indicating that the bridging hydroxide serves as the general base to activate the attacking water. This attack results in the penta-coordinate intermediate shown in Figure 4. The barrier and reaction energy for this step are calculated to be +17.3 and +13.3 kcal/mol, respectively. The barrier for the base mechanism is thus significantly higher than the previously calculated barrier where the bridging hydroxide is the nucleophile (11.7 kcal/mol, *9*). These findings thus provide additional evidence that the bridging hydroxide acts as a nucleophile and not as a general base in the Zn/Zn-PTE reaction.

Discussion

Enzyme-Product Complexes with PTE

The x-ray crystal structures of the diethyl phosphate product complex and an inhibitor complex with cacodylate have been determined with the phosphotriesterase from *P. diminuta*. The structures of these two complexes were determined in an attempt to provide experimental support for recent variations in the reaction mechanism that have been postulated for this enzyme (10,11). With the diethyl phosphate product, the ligand is found bridging the two divalent cations as illustrated in Figure 3. The two metal ions are separated by a distance of

4.0 Å, where one of the negatively charged phosphate oxygens of the product is 2.1 Å from the α-metal ion while the other oxygen is 1.9 Å from the β-metal ion. There are no water molecules associated with either metal within a distance of 5.4 Å. The distances between the two divalent cations and bound ligands for the various complexes are compared in Figure 5. The symmetrical bridge observed in this complex differs from the prediction of this structure based upon the calculations of Wong and Gao (10). They have postulated that the diethyl phosphate product would be bound asymmetrically to the binuclear metal center with exclusive coordination to the β-metal ion and a metal-metal separation of 5.3 Å. It is unclear from the structure determined here whether or not the carboxylate side chain of Asp-301 is protonated or not. However, the distance of the nearest carboxylate oxygen of Asp-301 is found 2.4 Å from the α-metal ion in the diethyl phosphate complex compared with a distance of 2.5 Å in the unliganded complex (8). The structure of diethyl phosphate bound to PTE determined here is consistent with the complex proposed by Aubert *et al.* (8). There is no indication that the two divalent cations can be separated by a distance that approaches the 5.3 Å predicted by Wong and Gao. The experimentally determined complex resembles that of a highly symmetric bridge with nearly equal distances between each metal ion and the nearest phosphate oxygen.

A nearly identical structure is observed for the G60A mutant in the complex with the cacodylate anion (Figure 3). The G60A mutant has nearly identical kinetic constants as the wild type enzyme for the hydrolysis of paraoxon but is more stereoselective for the hydrolysis of substrates with larger substituents attached to the phosphorus core (28). Cacodylate is an analogue of the diethyl phosphate product since it bears a single negative charge within a tetrahedral architecture. The coordination geometry of this ligand to the binuclear metal center is nearly symmetric with oxygen-metal distances of 2.0 and 2.1 Å to the α- and β-metal ions respectively. There are no water molecules coordinated to either metal within a distance of 3.0 Å.

The coordination geometries of the diethyl phosphate and cacodylate bound to the binuclear metal center of PTE are not consistent with the mechanism for phosphotriester hydrolysis proposed by Jackson *et al.* (11). For the phosphotriesterase isolated from *A. radiobacter* it has been postulated that the bridging hydroxide acts not as a nucleophile but as a general base in the abstraction of a proton from a water molecule coordinated to the α-metal ion. The primary experimental support for this conjecture stems from the determination of the structures of diethyl thiophosphate and dimethyl thiophosphate bound to the active site of the PTE from *A. radiobacter* (11,13). These structures reveal a bridging complex for either thiophosphate product plus the coordination of an additional bridging hydroxide. These complexes are consistent with the mechanism depicted in Scheme 3. However, to the best of our knowledge, there have been no crystal structures of PTE where the α-metal ion is 6-coordinate with an additional water molecule that could function as the primary nucleophile. Thus, experimental support for an additional water molecule that is activated by the bridging hydroxide is lacking. The identities of the metal ions bound to PTE from *A. radiobacter* are also different from the *P. diminuta* PTE. The structure of this enzyme was determined with Fe in the α-position and Zn in the β-position. Hexacoordinate zinc complexes are extremely rare and thus it seems quite unlikely that the Zn/Zn-PTE from *P. diminuta* could function in the manner as proposed by Ollis and coworkers. The DFT calculations presented here give further support to this conclusion. It was not possible to optimize a structure in which an additional water molecule is bound to the α-Zn and the barrier for the base mechanism is calculated to be significantly higher than the nucleophile mechanism.

Product Complexes in the Amidohydrolase Superfamily

X-ray crystal structures have been determined for other members of the amidohydrolase superfamily (1). It seems reasonable to assume that for those enzymes in this superfamily that

contain a binuclear metal center that many aspects of the chemical reaction mechanisms would be quite similar to one another. Structures of these enzymes, determined in the presence of their respective hydrolysis products, should illuminate whether or not the diethyl phosphate structure, determined for PTE, provides a common mechanistic or structural theme for the rest of the amidohydrolase superfamily.

Isoaspartyl dipeptidase (IAD) catalyzes the hydrolysis of amide bonds formed with the side chain carboxylate of aspartic acid (29). A 2.1 Å resolution structure of this enzyme has been determined in the presence of aspartate, the reaction product (30). A representation of the structure is illustrated in Figure 6 showing the bound aspartate. The carboxylate side chain is found bridging the two zinc atoms within the active site in a somewhat asymmetric arrangement. The two metal ions are separated by a distance of 3.8 Å. The carboxylate oxygen nearest the α-metal is separated by a distance of 2.8 Å while the other oxygen is 2.3 Å away from the β-metal ion. There are no other water molecules within 4.1Å of either metal ion. A similar complex is also observed in the structure of acetate bound within the active site of D-aminoacylase (Figure 6). This enzyme catalyzes the hydrolysis of the amide bond of *N*-acetyl-D-amino acid derivatives (31,32). This particular enzyme requires a divalent cation bound to the β-site but is less particular about the requirement for the occupancy of the metal ion at the α-site. In any event, the coordination of acetate to the active site shows that the two metal ions are 3.2 Å from one another. One of the oxygens of the bound acetate is 2.5 Å from the α-metal whereas the other oxygen is 2.0 Å from the β-metal. There are no other water molecules that are bound to either metal ion.

Dihydroorotase catalyzes the reversible interconversion of carbamoyl aspartate and dihydroorotate in the biosynthetic pathway for the assembly of pyrimidine nucleotides. When the structure of this enzyme was determined in the presence of added dihydroorotate it was found, quite remarkably, that in one subunit of the dimer dihydroorotate was bound, while in the adjacent subunit carbamoyl aspartate was bound. Thus the structure of this enzyme-substrate/product complex provided a nearly unprecedented view of the reaction immediately before and after the chemical reaction had been catalyzed. In the complex with the bound carbamoyl aspartate the two zinc atoms are separated by a distance of 3.7 Å. One of the carboxylate oxygens is 2.3 Å away from the α-metal ion while the other oxygen is 2.2 Å away from the β-metal ion (33). Thus, the bridging complex is symmetric and there are no other visible water molecules that could function as the nucleophile in the complex with dihydroorotate (Figure 6).

Conclusions

The structure of PTE from *P. diminuta* has been determined in the presence of the hydrolysis product diethyl phosphate and a product analogue, cacodylate. In either structure the complex is formed as a bridging ligand between the two divalent cations in a symmetric orientation where the average oxygen-metal distance is 2.0 Å. The average metal-metal separation in this complex is 3.9 Å, compared with 3.4 Å in the unliganded complex. In either structure there is no evidence for the additional binding of hydroxide to either of the two divalent cations. These results provide strong experimental support for the coordination geometry of the reaction product, originally postulated by Aubert *et al.* and illustrated in Scheme 2. The enzyme-product complex, predicted by Wong and Gao to be asymmetrically associated with only the β-metal ion coupled with a metal-metal separation of 5.3 Å, is not supported by these results (10). The structures presented in this paper are also at variance with the proposed mechanism postulated by Ollis and coworkers (11,13). In the complex with diethyl phosphate there is no evidence for the binding of an additional hydroxide as a bridging ligand between the two divalent cations. These results support the computational assessment of the reaction mechanism of PTE which concluded that the bridging hydroxide is sufficiently nucleophilic to attack the phosphorus

center of organophosphate triester substrates (9,10,34). The formation of product complexes with the simultaneous complexation of hydroxide and product in the active site of PTE from *A. radiobacter* are likely the result of iron occupying the α-metal ion site of that enzyme.

Supplementary Material

Refer to Web version on PubMed Central for supplementary material.

REFERENCES

1. Seibert CM, Raushel FM. Structural and catalytic diversity within the amidohydrolase superfamily. Biochemistry 2005;44:6383–6391. [PubMed: 15850372]
2. Benning MM, Shim H, Raushel FM, Holden HM. High resolution X-ray structures of different metal-substituted forms of phosphotriesterase from *Pseudomonas diminuta*. Biochemistry 2001;40:2712–2722. [PubMed: 11258882]
3. Donarski WJ, Dumas DP, Heitmeyer DP, Lewis VE, Raushel FM. Structure-activity relationships in the hydrolysis of substrates by the phosphotriesterase from *Pseudomonas diminuta*. Biochemistry 1989;28:4650–4655. [PubMed: 2548585]
4. Dumas DP, Durst HD, Landis WG, Raushel FM, Wild JR. Purification and properties of the phosphotriesterase for *Pseudomonas diminuta*. Arch. Biochem. Biophys 1990;277:155–159. [PubMed: 2154956]
5. Caldwell SR, Newcomb JR, Schlecht KA, Raushel FM. Limits of diffusion in the hydrolysis of substrates by the phosphotriesterase from *Pseudomonas diminuta*. Biochemistry 1991;30:7438–7444. [PubMed: 1649628]
6. Raushel FM, Holden HM. Phosphotriesterase: an enzyme in search of its natural substrate. Adv. Enzymol. Relat Areas Mol. Biol 2000;74:51–93. [PubMed: 10800593]
7. Omburo GA, Kuo JM, Mullins LS, Raushel FM. Characterization of the zinc binding site of bacterial phosphotriesterase. J. Biol. Chem 1992;267:13278–13283. [PubMed: 1320014]
8. Aubert SD, Li Y, Raushel FM. Mechanism for the hydrolysis of organophosphates by the bacterial phosphotriesterase. Biochemistry 2004;43:5707–5715. [PubMed: 15134445]
9. Chen S-L, Fang W-H, Himo F. Theoretical study of the phosphotriesterase reaction mechanism. J. Phys. Chem. B 2007;111:1253–1255. [PubMed: 17253743]
10. Wong K-Y, Gao J. The reaction mechanism of paraoxon hydrolysis by phosphotriesterase from combined QM/MM simulations. Biochemistry 2007;46:13352–13369. [PubMed: 17966992]
11. Jackson CJ, Foo JL, Kim HK, Carr PD, Liu JW, Salem G, Ollis DL. In crystallo capture of a Michaelis complex and product-binding modes of a bacterial phosphotriesterase. J. Mol. Biol 2008;375:1189–1196. [PubMed: 18082180]
12. Samples CR, Raushel FM, DeRose VJ. Activation of the binuclear metal center through formation of phosphotriesterase-inhibitor complexes. Biochemistry 2007;46:3435–3442. [PubMed: 17315951]
13. Jackson C, Kim HK, Carr PD, Liu JW, Ollis DL. The structure of an enzyme-product complex reveals the critical role of a terminal hydroxide nucleophile in the bacterial phosphotriesterase mechanism. Biochim Biophys Acta 2005;1752:56–64. [PubMed: 16054447]
14. Kuiper JM, Hulst R, Engberts JBFN. A selective and mild synthetic route to dialkyl phosphates. Synthesis 2003:695–698.
15. Otwinowski, Z.; Minor, W. Macromolecular crystallography, part A. In: Carter, CW., Jr.; Sweet, RM., editors. Methods in Enzymology. Academic Press; New York: 1997. p. 307-326.
16. Vagin A, Teplyakov A. MOLREP: an automated program for molecular replacement. J. Appl. Cryst 1997;30:1022–1025.
17. Lamzin, VS.; Wilson, KS.; Perrakis, A. Crystallography of biological macromolecules. In: Rossmann, MG.; Arnold, E., editors. International Tables for Crystallography. Dordrecht, Kluwer Academic Publishers; Dordrecht, The Netherlands: 2001. p. 720-722.
18. Emsley P, Cowtan K. Coot: model-building tools for molecular graphics. Acta Crystallographica Section D-Biological Crystallography 2004;60(Part 12 Sp Iss 1):2126–2132.

19. Murshudov GN, Vagin AA, Dodson EJ. Refinement of macromolecular structures by the maximum-likelihood method. Acta Cryst 1997;D53:240–255.

20. Becke AD. A new mixing of Hartree–Fock and local density-functional theories. J. Chem. Phys 1993;98:1372–1377.

21. Becke AD. Density-functional thermochemistry III. The role of exact exchange. J. Chem. Phys 1993;98:5648–5652.

22. Lee C, Yang W, Parr RG. Development of the Colle-Salvetti correlation-energy formula into a functional of the electron density. Phys. Rev. B 1988;37:785–789.

23. Barone V, Cossi M. Quantum calculation of molecular energies and energy gradients in solution by a conductor solvent model. J. Phys. Chem. A 1998;102:1995–2001.

24. Cammi R, Mennucci B, Tomasi J. Second-order Møller-Plesset analytical derivatives for the polarizable continuum model using the relaxed density approach. J. Phys. Chem. A 1999;103:9100–9108.

25. Klamt A, Schüürmann G. COSMO: a new approach to dielectric screening in solvents with explicit expressions for the screening energy and its gradient. J. Chem. Soc. Perkin. Trans 1993;2:799–800.

26. Tomasi J, Mennucci B, Cammi R. Quantum mechanical continuum solvation models. Chem. Rev 2005;105:2999–3094. [PubMed: 16092826]

27. Frisch, MJ.; Trucks, GW.; Schlegel, HB., et al. Gaussian 03, Revision D.01. Gaussian, Inc.; Wallingford CT: 2004.

28. Chen-Goodspeed M, Sogorb MA, Wu F, Hong S-B, Raushel FM. Structural determinants of the substrate and stereochemical specificity of phosphotriesterase. Biochemistry 2001;40:1325–1331. [PubMed: 11170459]

29. Martí-Arbona R, Fresquet V, Thoden JB, Davis ML, Holden HM, Raushel FM. Mechanism of the reaction catalyzed by isoaspartyl dipeptidase from *Escherichia coli*. Biochemistry 2005;44:7115–7124. [PubMed: 15882050]

30. Thoden JB, Marti-Arbona R, Raushel FM, Holden HM. High-resolution X-ray structure of isoaspartyl dipeptidase from *Escherichia coli*. Biochemistry 2003;42:4874–82. [PubMed: 12718528]

31. Liaw S-H, Chen S-J, Ko T-P, Hsu C-S, Chen C-J, Wang AH-J, Tsai Y-C. Crystal structure of d-aminoacylase from *Alcaligenes faecalis* DA1. J. Biol. Chem 2003;278:4957–4962. [PubMed: 12454005]

32. Lai W-L, Chou L-Y, Ting C-Y, Kirby R, Tsai Y-C, Wang AH-J, Liaw S-H. The functional role of the binuclear metal center in d-aminoacylase. J. Biol. Chem 2004;279:13962–13967. [PubMed: 14736882]

33. Thoden JB, Phillips GM, Neal TM, Raushel FM, Holden HM. Molecular structure of dihydroorotase: A paradigm for catalysis through the use of a binuclear metal center. Biochemistry 2001;40:6989–6997. [PubMed: 11401542]

34. Zheng F, Znan C-G, Ornstein RL. Theoretical determination of two structural forms of the active site in cadmium-containing phosphotriesterases. J. Phys. Chem. B 2002;106:717–722.

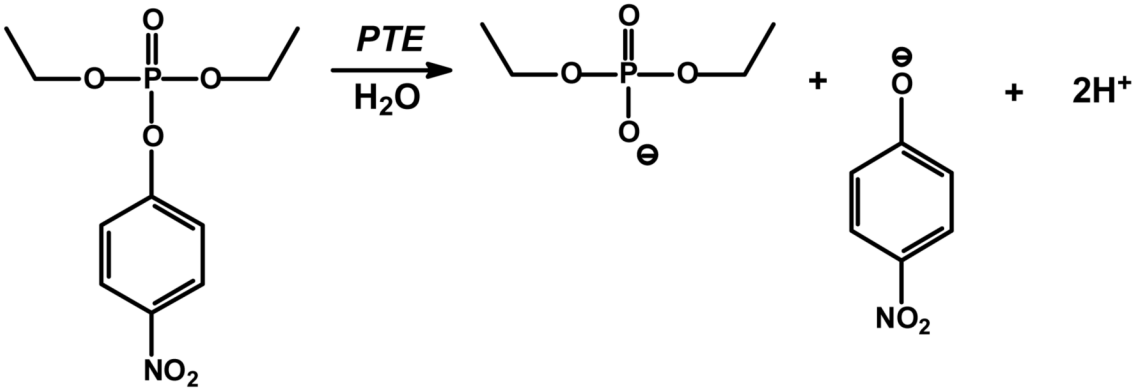

Scheme 1.

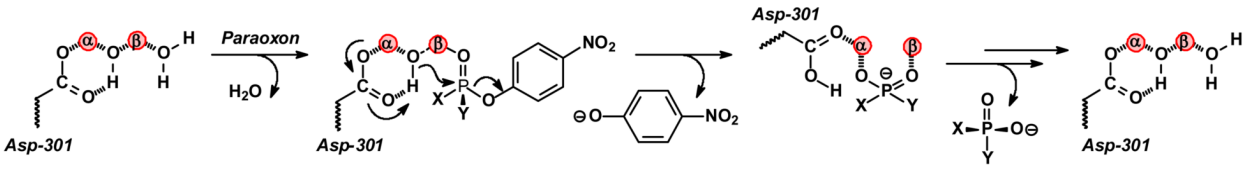

Scheme 2.

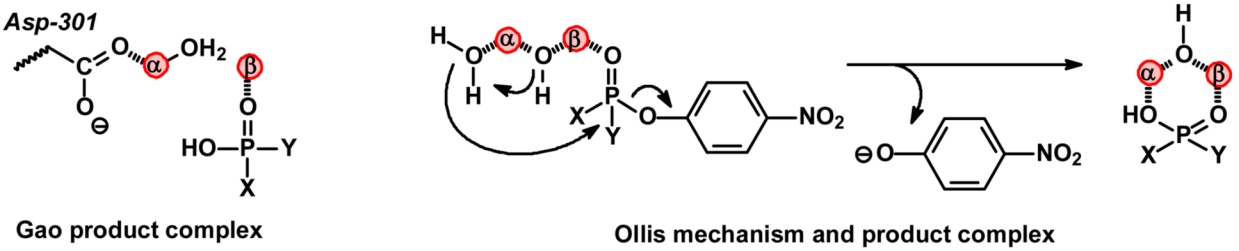

Scheme 3.

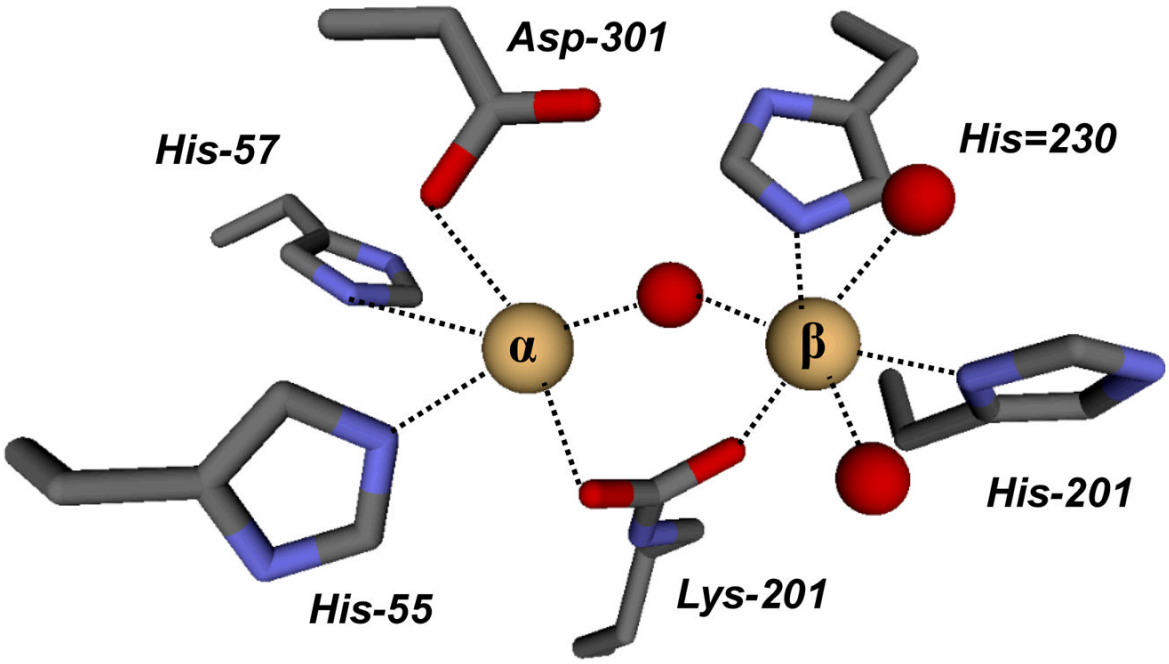

Figure 1.
A model for the structure of the binuclear metal center within the active site of Cd/Cd-PTE (2). The coordinates taken from PDB code: 1JGM. The two metal ions are depicted as light brown spheres.

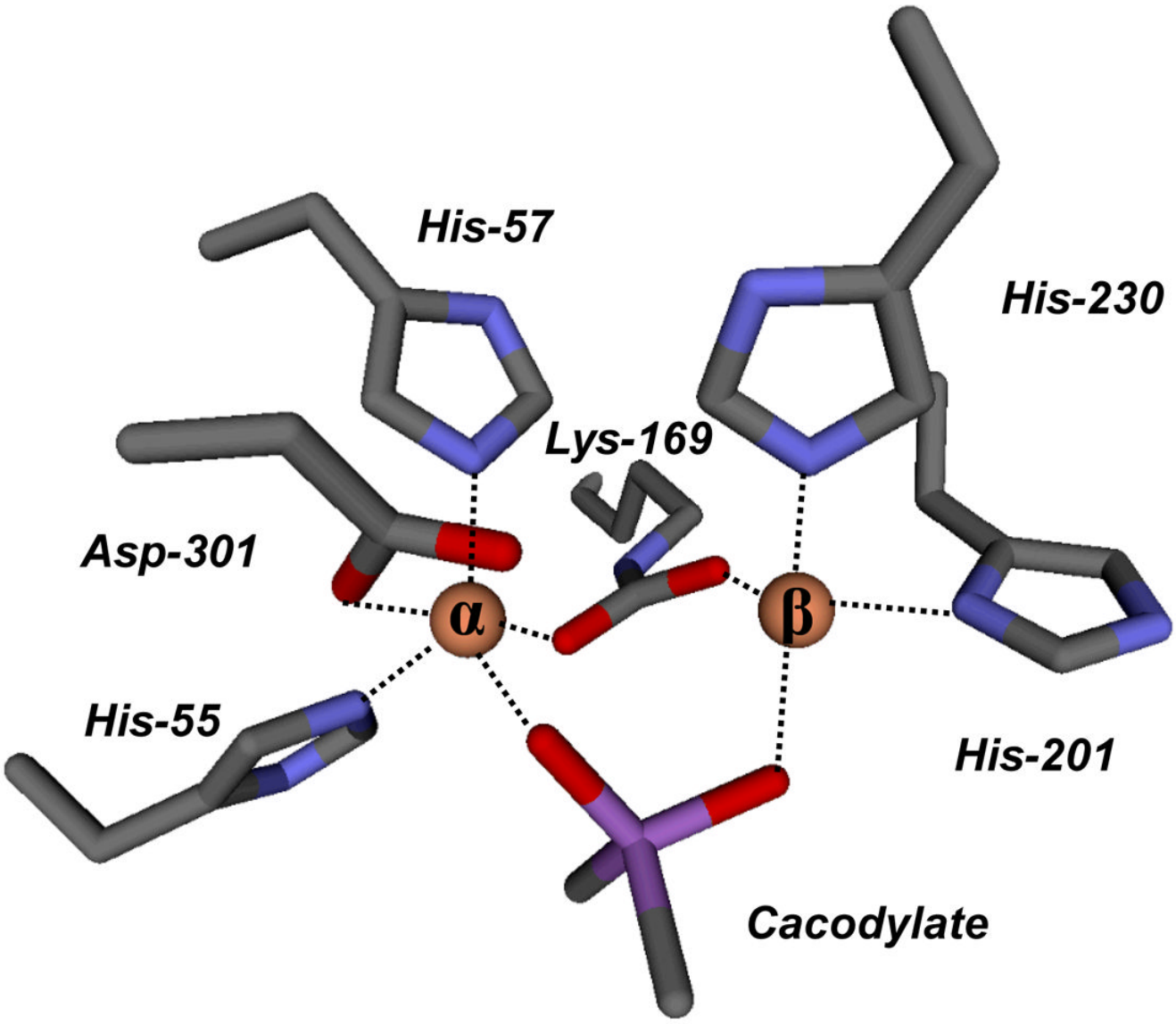

Figure 2.
A model for the active site of Co/Co-PTE (mutant G60A) obtained from crystals grown in the presence of cacodylate.

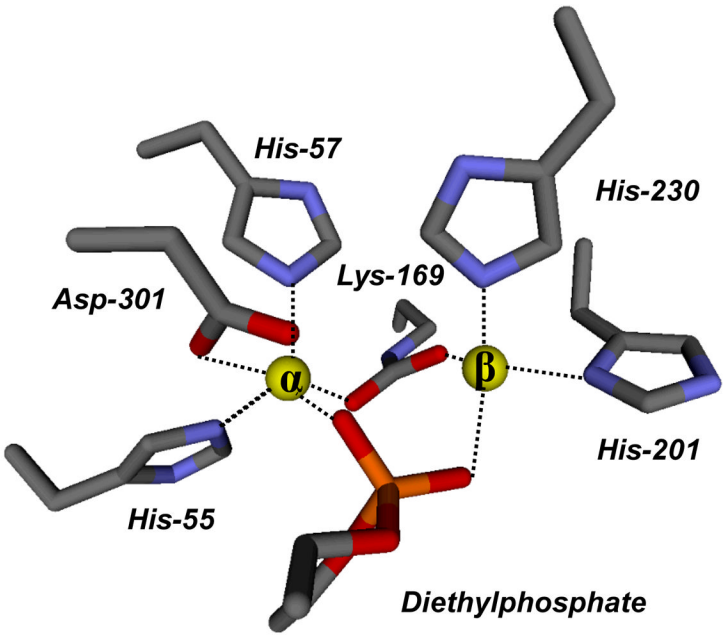

Figure 3.
A model for the active site of wild type Co/Co-PTE from crystals grown in the presence of diethylphosphate.

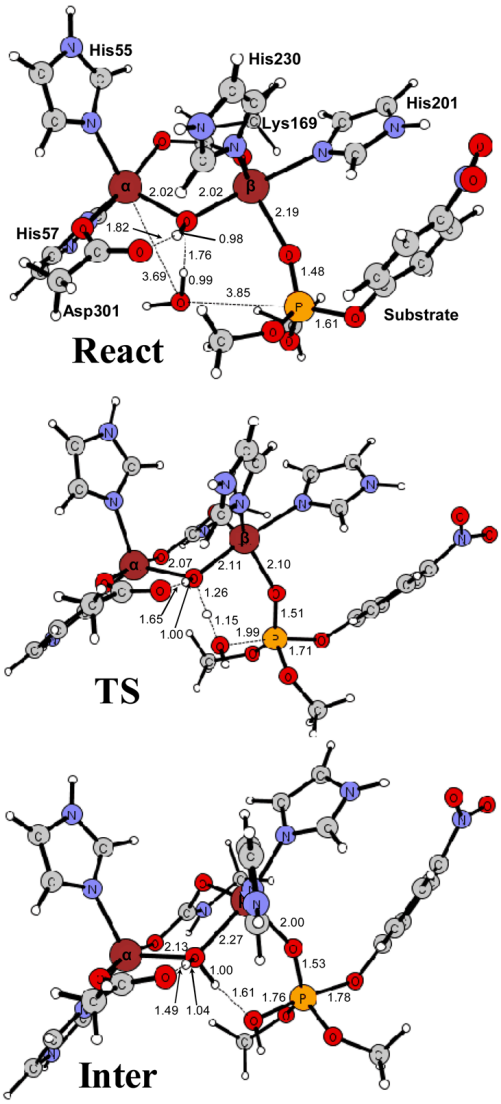

Figure 4.
Optimized geometries of the Zn/Zn-PTE active site model with dimethyl 4-nitrophenyl phosphate and a water molecule bound (**React**), the transition state for the water attack on the phosphorus (**TS**), and the resulting penta-coordinate intermediate (**Inter**). Distances are in angstrom (Å).

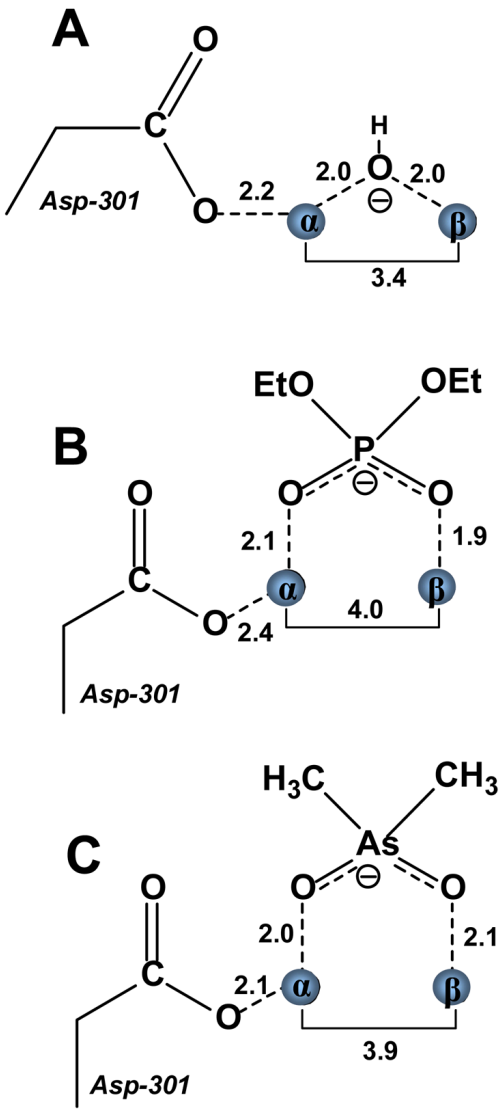

Figure 5.

Schematic representations of the binuclear metal centers of the binuclear metal centers from Co/Co-PTE in the presence and absence of diethylphosphate and cacodylate. (A) Zn/Zn-PTE in the absence of added ligands (PDB code: 1HZY). (B) Co/Co -PTE in the presence of added diethylphosphate (PDB code: 3CAK). (C) Co/Co -G60A PTE in the presence of cacodylate (PDB code: 2O4Q).

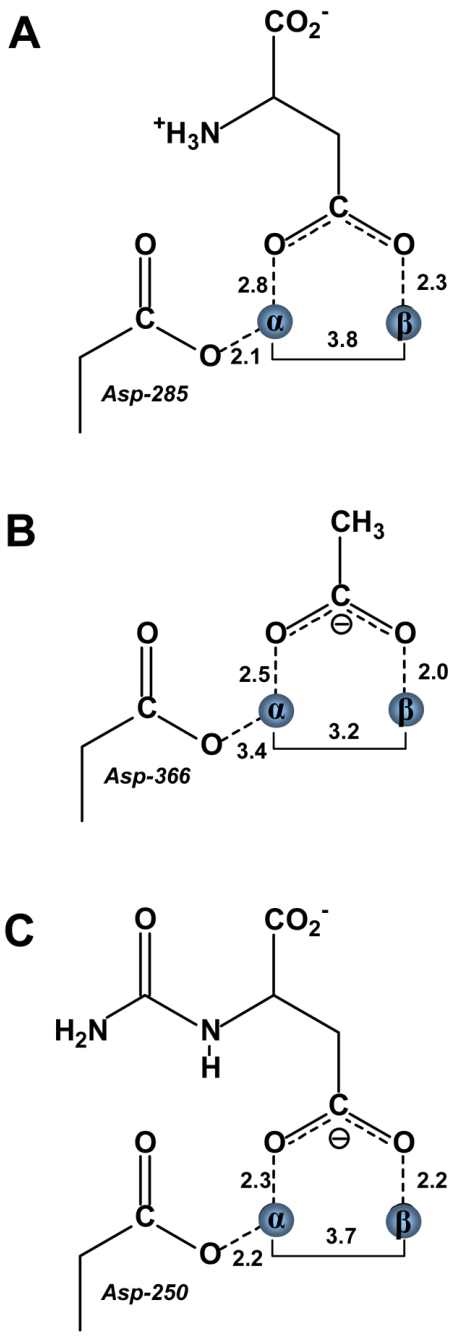

Figure 6.

Schematic representations of the binuclear metal centers for isoaspartyl dipeptidase, D-aminoacylase, and dihydroorotase in the presence of bound reaction products. (A) Isoaspartyl dipeptidase in the presence of aspartic acid (PDB code: 1ONX). (B) D-Aminoacylase in the presence of acetate (PDB code: 1M7J). (C) Dihydroorotase in the presence of carbamoyl aspartate (PDB code: 1J79).

Table 1

Data collection and refinement statistics

Data collection	**G60A-cacodylate**	**wild type PTE-DEP**
Resolution, Å	31.64-1.95	20.49-1.83
Observed reflections	270,828	137,406
Unique reflections	91,515	47,158
Completeness	96.3(80.7)[1]	93.2(81.8)[1]
I/sigma	15.8 (3.4)[1]	13.2 (3.0)[1]
Rmerge[2]	0.076(0.286)[1]	0.061(0.319)[1]
Refinement	**G60A-cacodylate**	**wild-type PTE-DEP**
Protein nonhydrogen atoms	10,161	5,116
Water molecules	1,163	843
R_{cryst}[3]	0.167	0.140
R_{free}[3]	0.224	0.196
Average B-factor, (Å^2)		
Main chain	20.5	13.1
Side chains	22.2	15.2
Waters	30.6	27.6
RMSD from ideal geometry		
Bond length, Å	0.014	0.014
Bond angles, (°)	1.5	1.4

[1] Values in parentheses correspond to highest resolution shell 2.02 to 1.95 Å for G60A, 1.90 to 1.83 Å for wild type PTE with DEP.

[2] $R_{merge} = \Sigma\Sigma j|Ij(hkl) - \langle I(hkl)\rangle|/\Sigma\Sigma j|\langle I(hkl)\rangle|$, where Ij is the intensity measurement for reflection j and <I> is the mean intensity over j reflections.

[3] $R_{cryst}/(R_{free}) = \Sigma||F_{obs}(hkl)| - |F_{calc}(hkl)||/\Sigma|F_{obs}(hkl)|$, where F_{obs} and F_{calc} are observed and calculated structure factors, respectively. No σ-cutoff was applied. 5% of the reflections were excluded from the refinement and used to calculate R_{free}.